

# X-MoS<sub>2</sub>/GO/Graphene Heterostructures and Doping Effects: KPFM Based Study of Surface Potential

Diogo José Horst<sup>1,\*</sup> , Rogério de Almeida Vieira<sup>1</sup>, Alejandra García-García<sup>2</sup>,  
Alejandra Moreno-Barcenas<sup>2</sup>

<sup>1</sup> Department of Chemistry, Federal University of São Paulo – UNIFESP, Brazil

<sup>2</sup> Laboratory for Synthesis and Modification of Nanostructures and M2D - CIMAV S.C., Mexico

\* Correspondence: diogohorst@gmail.com;

Scopus Author ID 55823621400

Received: 5.10.2023; Accepted: 29.01.2024; Published: 21.07.2024

**Abstract:** In this work, we report the contact potential difference measured by Kelvin probe force microscopy of phosphorus-doped Si/MoS<sub>2</sub>/graphene and Si/MoS<sub>2</sub>/GO with different thicknesses deposited using micro drop casting and chemical vapor deposition. Doping with 15% phosphorus increased the surface potential of the layers. The readings obtained were from -722.27 to +340.46, showing that layer orientation is equally important as layer thickness when designing multilayer two-dimensional systems where surface potential is considered. The number of layers is essential to forming metal contacts for fabricating future MoS<sub>2</sub>-GO-based devices.

**Keywords:** graphene/MoS<sub>2</sub>; GO/MoS<sub>2</sub>; heterostructures; superficial potential; Kelvin probe force microscopy.

© 2024 by the authors. This article is an open-access article distributed under the terms and conditions of the Creative Commons Attribution (CC BY) license (<https://creativecommons.org/licenses/by/4.0/>).

## 1. Introduction

The various 2D materials' qualities make them attractive candidates for a wide range of applications, which is why there is so much interest in them. Furthermore, the creation of composite, on-demand materials known as van der Waals heterostructures—which capitalize on the properties of those materials to produce functions that would not otherwise be possible—is made possible by combining 2D crystals. For instance, the precise mixing of 2D materials creates new avenues for investigating novel applications [1-5].

Molybdenum disulfide and graphene as representative 2D materials have been widely studied recently. Its special physical and chemical properties have attracted interest in them. The combination of bidimensional materials may offer new application opportunities due to their synergistic properties[6-10].

At present, MoS<sub>2</sub>-based heterostructures as building blocks have been studied. The MoS<sub>2</sub>/graphene and analog heterostructures are a hot research issue today.

Van der Waals (VdW) heterostructures have been proposed to modify two-dimensional layered materials with desired properties, thus greatly extending the applications of these materials [11-13]. By combining MoS<sub>2</sub>/graphene or MoS<sub>2</sub>/GO, higher electron transfer to MoS<sub>2</sub> can be obtained, giving advantages for many applications [14]. Some works have reported an improved sensing performance of these materials [15-18]. Including the electrochemical performance of phosphorus-doped graphene/MoS<sub>2</sub> [19- 22].

In a recent study, Rana *et al.* (2023) [23] showed MoS<sub>2</sub> and rGO nanocomposites-based electrochemical sensors for detecting mercury ions.

In another study, Le *et al.* (2023) [24] developed a hybrid nanofluid containing graphene oxide and molybdenum disulfide nanoparticles with engine oil-based fluid. This shows that the synergy of the two materials shows promise for various applications.

In this study, we investigate the electronic potential of phosphorous-doped MoS<sub>2</sub>/graphene and MoS<sub>2</sub>/Go heterostructures using the Kelvin Probe Field Microscopy technique.

## 2. Materials and Methods

### 2.1. Molybdenum disulfide synthesis.

The synthesis of MoS<sub>2</sub> was carried out in the register under patent MX-a-2017-016742. The raw materials were MoO<sub>3</sub> and sulfur powder; these were put into a tube furnace at 600°C under N<sub>2</sub> flow. Afterward, a post-treatment via recrystallization was performed at 800°C for 1 h. After the sulfurization and recrystallization processes, the furnace was left to cool down to room temperature under N<sub>2</sub> flow, and the final MoS<sub>2</sub> powder was obtained.

For doped MoS<sub>2</sub> synthesis, a dopant precursor was introduced during the growth step and mixed with sulfur powder at two different concentrations (5 and 15% phosphorous).

### 2.2. Graphene oxide synthesis.

All the chemical reagents used to synthesize GO were purchased from Sigma-Aldrich. For the synthesis of GO, the mineral graphite was the raw material, while sulphuric acid (H<sub>2</sub>SO<sub>4</sub>, >95%), nitric acid (HNO<sub>3</sub>, 68–70%), and potassium permanganate (KMnO<sub>4</sub>, >97%) were the oxidant reagents. For the synthesis, graphite was added to a concentrated solution of H<sub>2</sub>SO<sub>4</sub>/HNO<sub>3</sub> (volume ratio 3:1) according to the methodology registered by the group of synthesis and modification of nanostructures and bidimensional materials. This mixture was sonicated for 30 minutes at a constant temperature before the oxidation process began. Potassium permanganate was added at a ratio of 1:7 concerning the mass of graphite. The solution was heated to 70°C and stirred for 24 hours. Finally, hydrogen peroxide was added to the solution to stop the oxidation process, and it was washed with deionized water until pH = 7. The niobium oxide was obtained from CBMM and was used without purification.

### 2.3. Graphene and niobium oxide deposition.

The graphene and niobium deposition was carried out in an RT-CVD from Annealsys with the beginning conditions from previous investigations and adjustments for copper electrodes as substrate. High-purity nitrogen, hydrogen, and methane gases were added to the growth process at  $1 \times 10^{-2}$  Torr pressure. The growth process begins when the temperature is raised to 950°C. An atmosphere of methane (10 sccm) mixed with 1000 sccm of nitrogen and hydrogen was necessary for film growth. The growth time was 15 minutes; after this time, the cooling step was carried out from 950°C to room temperature (RT).

### 2.4. Heterostructures obtention by single droplet assembly.

In this assay, 1 micro drop (2 μL) containing colloidal suspensions of pure MoS<sub>2</sub> and with phosphorus doping at 5 and 15% and GO (liquid-liquid phase) was dripped on plates of polished

crystalline silicon and also copper measuring approximately 1 x 1 cm. Previously, MoS<sub>2</sub> and GO nanoparticles were added to 5 ml of deionized H<sub>2</sub>O and 200 μL of ethanol for dilution. The aqueous suspension was sonicated for 20 minutes to homogenize the mixture. The microdrop was deposited using a micropipette, and for evaporation of the colloidal suspension, the Si and Cu plates were heated at 100–120°C for 1–3 minutes (SHI *et al.*, 2020). After evaporating the solvent, the sediments were deposited on the plate, obtaining depositions of superimposed monolayer films of Si+MoS<sub>2</sub>+GO and Si+MoS<sub>2</sub>+ monolayer graphene, and Cu+MoS<sub>2</sub>+GO and Cu+MoS<sub>2</sub>+monolayer graphene.

*2.5. Heterostructures obtained by chemical vapor deposition.*

The films were synthesized on SiO<sub>2</sub>/Si and Cu substrates in a blast furnace, and some samples were doped with 5% and 15% phosphorus to verify their energy potential. The depositions were performed on silicon plates (1 x 1 cm) using a quartz tube oven (Lindberg Blue M, Thermo Scientific). Subsequently, graphene and niobium layers were deposited on the copper electrodes using a fast thermal processor (RTP-system, AS-micro Annealsys) with preheating at 750°C and reaching 950°C in a quartz tube using several gases with the following control parameters: N<sub>2</sub> (1000 ccm), H<sub>2</sub> (10 ccm), and CH<sub>4</sub> (5 ccm).

Figure 1 shows the graphical representation of layered depositions and analysis procedures:

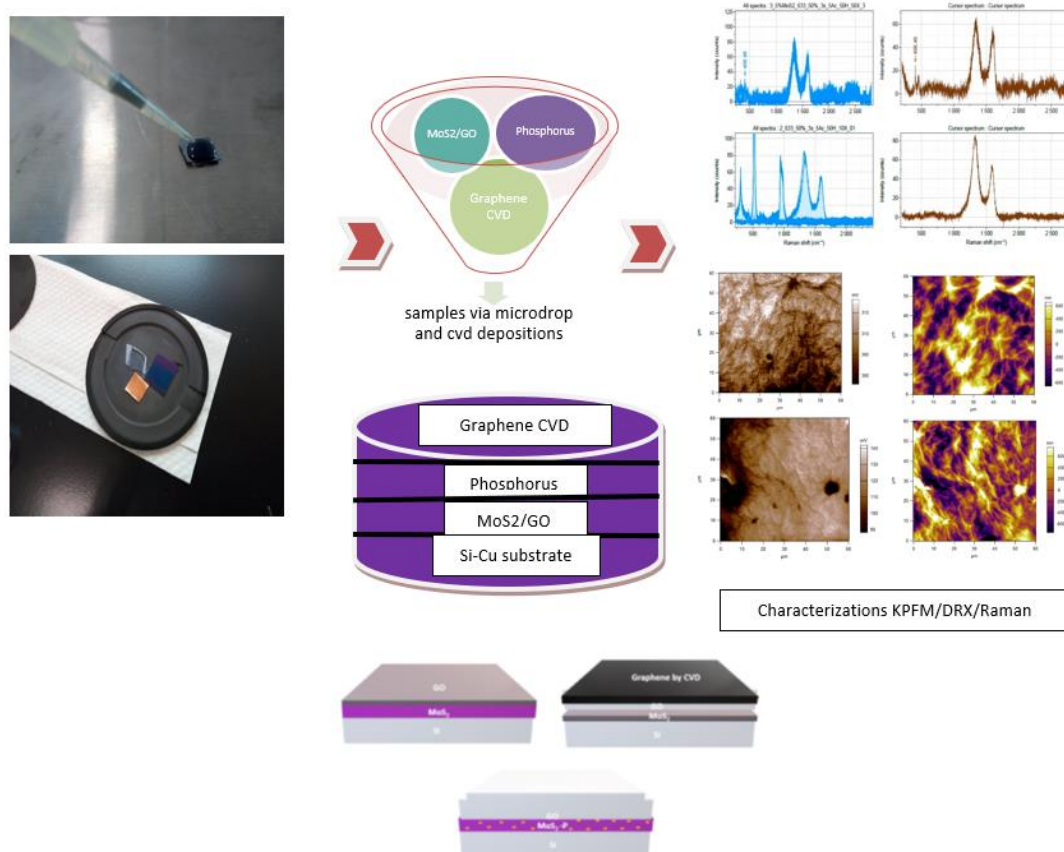


**Figure 1.** Graphical representation of the deposited layers and analysis procedures.

**3. Results and Discussion**

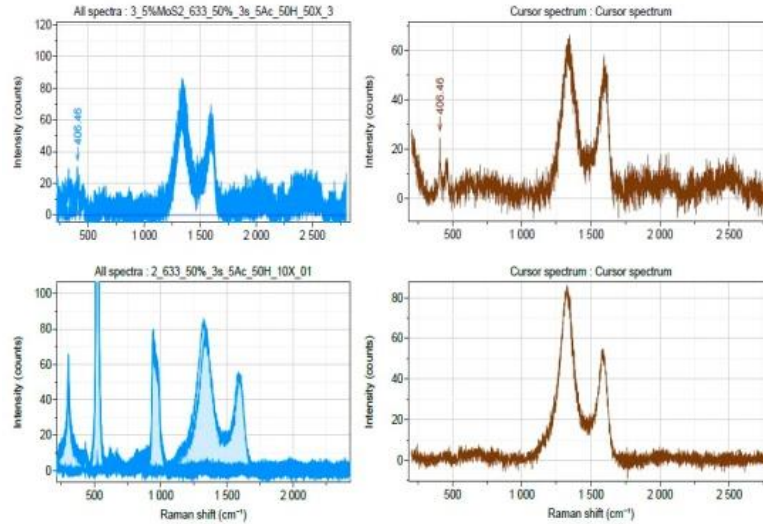
With quantitative information from KPFM, a profile across the scratching channel between the heterostructures deposited over the Si substrate was made. KPFM profiles were

collected from different positions for the same sample. The contact potential difference (CPD) between the tip and sample surface can be defined as follows:

$$CPD = \varphi_t - \varphi_s/e \quad (1)$$

Where  $\varphi_t$  and  $\varphi_s$  are the work functions of the conductive AFM tip and sample, respectively, and  $e$  is the elementary charge [15].

Figure 2 shows the Raman spectrum of samples:

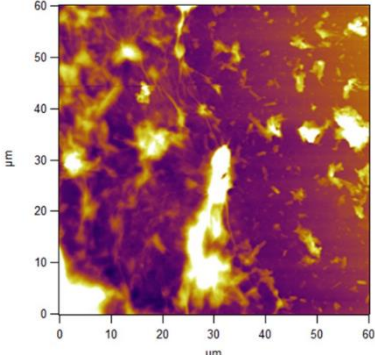
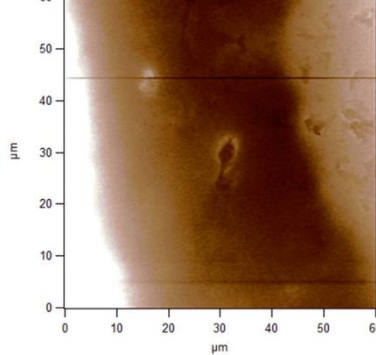
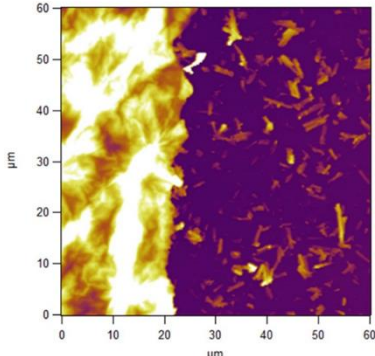
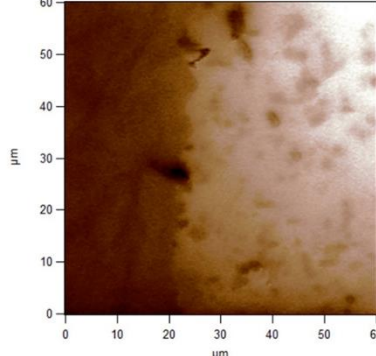
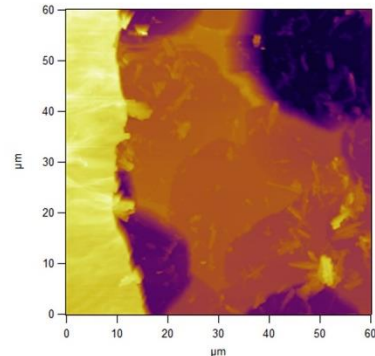
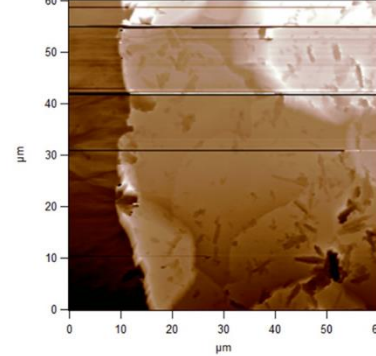
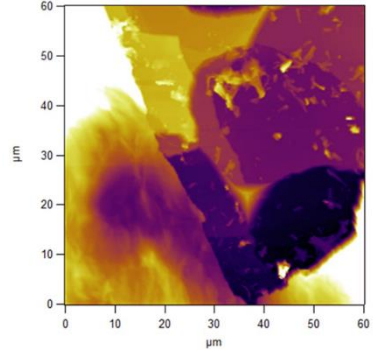
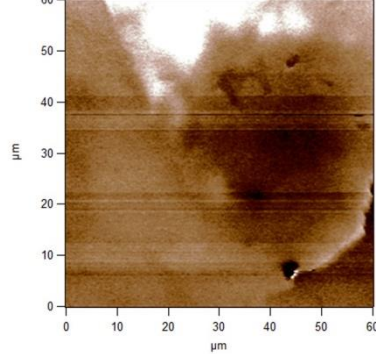


**Figure 2.** Raman spectrum of the sample.

Table 1 presents the surface potential mapping of the KPFM analysis for the studied samples:

**Table 1.** Surface potential mapping using KPFM

Sample	Morphology	CPD	CPD (mV)
MoS <sub>2</sub> /GO			+233.04
MoS <sub>2</sub> /GO/GCVD			+109.3

<p><b>5%<sub>dop</sub>- MoS<sub>2</sub>/GO</b></p>			<p>+153.43</p>
<p><b>15%<sub>dop</sub>- MoS<sub>2</sub>/GO</b></p>			<p>+340.46</p>
<p><b>5%<sub>dop</sub>- MoS<sub>2</sub>/GO/GcVD</b></p>			<p>-722.27</p>
<p><b>15%<sub>dop</sub>- MoS<sub>2</sub>/GO/GcVD</b></p>			<p>+189.63</p>

In similar research, Panchal *et al.* (2013) [26] found values of VCPD1-2LG = 150 mV for the surface potential measurements of graphene domains. Also, corroborating with the results found by Wang *et al.* (2023) [27] for values including 5% phosphorus doping.

According to Robinson *et al.* (2018) [28], variations in graphene's Fermi energy, or charge carrier density, induce shifts in the Raman G peak position ( $\Gamma$ G). Fundamentally, deviations in  $\Gamma$ G result from electron-phonon coupling and bond stiffness changes. Already for molybdenum disulfide, the Fermi energy variations were recently studied and described by Jones *et al.* (2022) [29].

According to Kumar *et al.* (2016) [30], the main peak (A) at  $\approx 185$  mV corresponds to VOC values obtained from the graphene layer, and the lower intensity peak (B) corresponds to a lower value of VOC ( $\approx 160$  mV) at points lying on defect regions. The same was verified in this study. Lower VOC regions are not desirable and are responsible for an overall decrease in the performance of devices. Therefore, it is important to investigate the local factors responsible for VOC variations. Similar values were recently found and described in research by Bangu *et al.* (2023) [31] when analyzing MoS<sub>2</sub>/graphene composites.

#### 4. Conclusions

Molybdenum disulfide (MoS<sub>2</sub>) is a favorable candidate to be combined with several carbon-derived nanomaterials to obtain new hybrid nanostructures with excellent physicochemical and electronic properties. The design and production of new two-dimensional heterostructures using modern techniques present a promising perspective for current nanotechnology.

The combination of two highly versatile materials, graphene oxide and molybdenum disulfide, forms layered GO-MoS<sub>2</sub> hybrids that present great potential for detection applications such as sensors.

While graphene is chemically inert as it is a gapless semimetal, its iso-structural analog MoS<sub>2</sub> is chemically versatile with band gaps, thus finding significant use in many applications. Therefore, designing the structure and/or density of boundary and grain boundaries into 2D materials is a promising way to customize their performance. Grain boundary boundaries in two-dimensional material layers impact their electrical properties, optoelectronics, and mechanics.

Therefore, it is worth investigating the availability of simple approaches for synthesizing and characterizing these 2D heterostructures. This work aimed to study the synthesis and characteristics of two-dimensional heterostructures (2D/2D) using pure molybdenum disulfide (MoS<sub>2</sub>) and doped with phosphorus at 5 and 15% combined with graphene oxide and graphene CVD. These heterostructures were deposited on silicon and copper substrates via micro drop and CVD.

The chemical and structural information of the samples were evaluated by Raman spectroscopy, Energy Scattering X-ray Spectroscopy (EDS), Scanning Electron Microscopy (SEM), and Kelvin Probe Force Microscopy (KPFM). The results prove the synergy between the materials, resulting in electronic coupling and making this system potentially applicable to electronic devices. The two methodologies studied proved to be viable: the deposition of MoS<sub>2</sub>+GO in the liquid-liquid phase, the microdroplet deposition technique proved to be simple and practical, presenting ease of replication, and the deposition in the solid-liquid phase (graphene+MoS<sub>2</sub>) presented the deposition of good quality graphene.

The Raman spectrum revealed peaks at 1350 and 1588 cm<sup>-1</sup> for the D and G bands due to phosphorous doping of MoS<sub>2</sub>/GO. The D band corresponds to the scattering of defects or local disturbances present in the carbon, and the G bands originate from the tangential elongation in the plane of the C–C bonds in the graphitic structure. MoS<sub>2</sub> exhibited characteristic bands at 379 and 406 cm<sup>-1</sup>, corresponding to the first order E<sub>1</sub>2g and A<sub>1</sub>g mode of the 2H phase.

The atomic element concentration was C 70.82%, O 18.25%, S 3.74%, Si 5.77%, Mo 1.41%, and the mass concentration of the elements was in the order of C 54.53%, O 18.72%, S 7.69%, Si 10.39%, and Mo 8.67%.

The morphological analysis revealed the growth of MoS<sub>2</sub> crystals in the shapes of rods, nano-flowers, and pyramids and good formation in the graphene grain boundary.

KPFM analysis revealed that the number of layers deposited was from 1 to 10, with the band shift characterized by an interfacial dipole at the vertical MoS<sub>2</sub>/GO junction. Surface PV images reveal some surface defects and show the material is between  $-21.0$  meV and  $3.66$  V.

## Funding

This research received no external funding.

## Acknowledgments

The authors thank the Federal University of São Paulo (UNIFESP) Brazil and the Center for Research in Advanced Materials (CIMAV) Mexico for the laboratories and reagents.

## Conflicts of Interest

The authors declare no conflict of interest.

## References

1. Ares, P.; Novoselov, K.S. Recent advances in graphene and other 2D materials. *Nano Mater. Sci.* **2022**, *4*, 3-9, <https://doi.org/10.1016/j.nanoms.2021.05.002>.
2. Antidormi, A.; Colombo, L.; Roche, S. Emerging properties of non-crystalline phases of graphene and boron nitride based materials. *Nano Mater. Sci.* **2022**, *4*, 10-17, <https://doi.org/10.1016/j.nanoms.2021.03.003>.
3. Ismail, K.B.M.; Arun Kumar, M.; Mahalingam, S.; Kim, J.; Atchudan, R. Recent Advances in Molybdenum Disulfide and Its Nanocomposites for Energy Applications: Challenges and Development. *Materials* **2023**, *16*, 4471, <https://doi.org/10.3390/ma16124471>.
4. Feng, C.; Wu, W.; Liu, H.; Wang, J.; Wan, H.; Ma, G.; Wang, H. Emerging Opportunities for 2D Materials in Neuromorphic Computing. *Nanomaterials* **2023**, *13*, 2720, <https://doi.org/10.3390/nano13192720>.
5. Cheng, Y.; Wan, R.; Li, L.; Liu, Z.; Yan, S.; Li, L.; Wang, J.; Gao, Y. Research progress on improving the performance of MoS<sub>2</sub> photodetector. *J. Opt.* **2022**, *24*, 104003, <https://doi.org/10.1088/2040-8986/ac8a5b>.
6. Zhang, Z.-W.; Yang, Y.; Wu, H.; Zhang, T. Advances in the two-dimensional layer materials for cancer diagnosis and treatment: unique advantages beyond the microsphere. *Front. Bioeng. Biotechnol.* **2023**, *11*, 1278871, <https://doi.org/10.3389/fbioe.2023.1278871>.
7. Wang, G.; Hou, H.; Yan, Y.; Jagatramka, R.; Shirsalimian, A.; Wang, Y.; Li, B.; Daly, M.; Cao, C. Recent advances in the mechanics of 2D materials. *Int. J. Extrem. Manuf.* **2023**, *5*, 032002, <https://doi.org/10.1088/2631-7990/acda2>.
8. Naikoo, G.A.; Arshad, F.; Almas, M.; Hassan, I.U.; Pedram, M.Z.; Aljabali, A.A.A.; Mishra, V.; Serrano-Aroca, Á.; Birkett, M.; Charbe, N.B.; Goyal, R.; Negi, P.; El-Tanani, M.; Tambuwala, M.M. 2D materials, synthesis, characterization and toxicity: A critical review. *Chem.-Biol. Interact.* **2022**, *365*, 110081, <https://doi.org/10.1016/j.cbi.2022.110081>.
9. Ryu, B.; Wang, L.; Pu, H.; Chan, M.K.Y.; Chen, J. Understanding, discovery, and synthesis of 2D materials enabled by machine learning. *Chem. Soc. Rev.* **2022**, *51*, 1899-1925, <https://doi.org/10.1039/D1CS00503K>.
10. Zhang, X.; Lai, J.; Gray, T. Recent progress in low-temperature CVD growth of 2D materials. *Oxf. Open Mater. Sci.* **2023**, *3*, itad010, <https://doi.org/10.1093/oxfmat/itad010>.
11. Peng, Q.; Wang, Z.; Sa, B.; Wu, B.; Sun, W. Blue Phosphorene/MS<sub>2</sub> (M = Nb, Ta) Heterostructures As Promising Flexible Anodes for Lithium-Ion Batteries. *Appl. Mater. Interfaces* **2016**, *8*, 13449-13457, <https://doi.org/10.1021/acsami.6b03368>.
12. Hu, Z.; Liu, Q.; Chou, S.-L.; Dou, S.-X. Two-Dimensional Material-Based Heterostructures for Rechargeable Batteries. *Cell Rep. Phys. Sci.* **2021**, *2*, 100286, <https://doi.org/10.1016/j.xcrp.2020.100286>.
13. Ma, J.; Yuan, Y.; Sun, P. Performances enhancement of graphene/n-Si Schottky junction solar cells with dual-functional MoS<sub>2</sub> interfacial layers. *J. Alloys Compd.* **2021**, *883*, 160898, <https://doi.org/10.1016/j.jallcom.2021.160898>.

14. Nawz, T.; Safdar, A.; Hussain, M.; Sung Lee, D.; Siyar, M. Graphene to Advanced MoS<sub>2</sub>: A Review of Structure, Synthesis, and Optoelectronic Device Application. *Crystals* **2020**, *10*, 902, <https://doi.org/10.3390/cryst10100902>.
15. Du, Y.-T.; Kan, X.; Yang, F.; Gan, L.-Y.; Schwingenschlögl, U. MXene/Graphene Heterostructures as High-Performance Electrodes for Li-Ion Batteries. *ACS Appl. Mater. Interfaces* **2018**, *10*, 32867–32873, <https://doi.org/10.1021/acsami.8b10729>.
16. Tang, Y.; Li, H.; Mao, X.; Xie, J.; Lee, J.Y.; Fu, A. Bidirectional heterostructures consisting of graphene and lateral MoS<sub>2</sub>/WS<sub>2</sub> composites: a first-principles study. *RSC Adv.* **2019**, *9*, 34986-34994, <https://doi.org/10.1039/C9RA05692K>.
17. Li, J.; Luo, X. Tunable bandgap of graphene/MS<sub>2</sub> (M=W, Mo) heterobilayers for photovoltaic materials. *Mater. Res. Express* **2019**, *6*, 1250k7, <https://doi.org/10.1088/2053-1591/ab5198>.
18. Guo, J.; Xu, X.; Hill, J.P.; Wang, L.; Dang, J.; Kang, Y.; Li, Y.; Guan, W.; Yamauchi, Y. Graphene-carbon 2D heterostructures with hierarchically-porous P,N-doped layered architecture for capacitive deionization. *Chem. Sci.* **2021**, *12*, 10334-10340, <https://doi.org/10.1039/D1SC00915J>.
19. Langer, R.; Błoński, P.; Hofer, C.; Lazar, P.; Mustonen, K.; Meyer, J.C.; Susi, T.; Otyepka, M. Tailoring Electronic and Magnetic Properties of Graphene by Phosphorus Doping. *ACS Appl. Mater. Interfaces* **2020**, *12*, 34074-34085, <https://doi.org/10.1021/acsami.0c07564>.
20. Subramanian, S.; Xu, K.; Wang, Y.; Moser, S.; Simonson, N.A.; Deng, D.; Crespi, V.H.; Fullerton-Shirey, S.K.; Robinson, J.A. Tuning transport across MoS<sub>2</sub>/graphene interfaces via as-grown lateral heterostructures. *npj 2D Mater. Appl.* **2020**, *4*, 9, <https://doi.org/10.1038/s41699-020-0144-0>.
21. Muhammad, N.; Muzaffar, M.U.; Ding, Z.J. Black phosphorene/blue phosphorene van der Waals heterostructure: a potential anode material for lithium-ion batteries. *Phys. Chem. Chem. Phys.* **2021**, *23*, 17392-17401, <https://doi.org/10.1039/D1CP01509E>.
22. Sarmah, D.; Kumar, A. Symmetric Supercapacitors with layer-by-layer Molybdenum disulfide - reduced graphene oxide structures and poly(3,4-ethylenedioxythiophene) nanoparticles nanohybrid electrode. *J. Energy Storage* **2021**, *35*, 102289, <https://doi.org/10.1016/j.est.2021.102289>.
23. Rana, D.S.; Sharma, R.; Kumar, S.; Gupta, N.; Thakur, S.; Thakur, K.K.; Singh, D. Molybdenum disulfide (MoS<sub>2</sub>) and reduced graphene oxide (rGO) nanocomposite based electrochemical sensor for detecting mercury(II) ions. *Nano-Struct. Nano-Objects.* **2023**, *36*, 101041, <https://doi.org/10.1016/j.nanoso.2023.101041>.
24. Le, Q.H.; Ali, Q.; Al-Khaled, K.; Amir, M.; Riaz, S.; Ullah Khan, S.; Abdelmalek, Z.; Tlili, I. Study of hybrid nanofluid containing graphene oxide and molybdenum disulfide nanoparticles with engine oil base fluid: A non-singular fractional approach. *Ain Shams Eng. J.* **2024**, *15*, 102317, <https://doi.org/10.1016/j.asej.2023.102317>.
25. Zheng, Z.; An, J.; Gong, R.; Zeng, Y.; Ye, J.; Yu, L.; Florea, I.; Roca i Cabarrocas, P.; Chen, W. Coupled Investigation of Contact Potential and Microstructure Evolution of Ultra-Thin AlO<sub>x</sub> for Crystalline Si Passivation. *Nanomaterials* **2021**, *11*, 1803, <https://doi.org/10.3390/nano11071803>.
26. Panchal, V.; Pearce, R.; Yakimova, R.; Tzalenchuk, A.; Kazakova, O. Standardization of surface potential measurements of graphene domains. *Sci. Rep.* **2013**, *3*, 2597, <https://doi.org/10.1038/srep02597>.
27. Wang, W.; Qi, J.; Zhai, L.; Ma, C.; Ke, C.; Zhai, W.; Wu, Z.; Bao, K.; Yao, Y.; Li, S.; Chen, B.; Repaka, D.V.M.; Zhang, X.; Ye, R.; Lai, Z.; Luo, G.; Chen, Y.; He, Q. Preparation of 2D Molybdenum Phosphide via Surface-Confined Atomic Substitution. *Adv. Mater.* **2022**, *34*, 2203220, <https://doi.org/10.1002/adma.202203220>.
28. Robinson, J.T.; Culbertson, J.; Berg, M.; Ohta, T. Work Function Variations in Twisted Graphene Layers. *Sci. Rep.* **2018**, *8*, 2006, <https://doi.org/10.1038/s41598-018-19631-4>.
29. Jones, L.O.; Sadhukhan, T.; Schatz, G.C. Localized  $\pi$  Surface States on 2D Molybdenum Disulfide from Carbene-Functionalization as a Qubit Design Strategy. *ACS Phys. Chem. Au* **2022**, *2*, 277–281, <https://doi.org/10.1021/acspchemau.1c00055>.
30. Kumar, R.; Varandani, D.; Mehta, B.R. Nanoscale interface formation and charge transfer in graphene/silicon Schottky junctions; KPFM and CAFM studies. *Carbon* **2016**, *98*, 41-49, <https://doi.org/10.1016/j.carbon.2015.10.075>.
31. Bongu, C.S.; Krishnan, M.R.; Soliman, A.; Arsalan, M.; Alsharaeh, E.H. Flexible and Freestanding MoS<sub>2</sub>/Graphene Composite for High-Performance Supercapacitors. *ACS Omega* **2023**, *8*, 36789-36800, <https://doi.org/10.1021/acsomega.3c03370>.